Microstructural characterisation of a prototype titanium alloy structure processed via Direct Laser Deposition (DLD)

D. Clark[#], M.T. Whittaker * and M.R. Bache*

[#] Rolls-Royce plc, P.O. Box 31, Derby, UK, DE24 8BJ

* Materials Research Centre, School of Engineering, Swansea University, Singleton Park, Swansea, UK, SA2 8PP

Abstract

Processing trials have produced a three dimensional, thin-walled structure of representative aerospace component geometry, fabricated directly by laser melting of Ti 6Al4V powder. This additive-built form has been subjected to metallographic characterisation. The fabrication technique is evaluated as an economic, commercial process capable of adding features such as bosses or flanges as a hybrid-manufacturing route for existing forms of gas turbine components.

Samples were extracted from six locations with different wall thickness, varying form and intersecting ligament geometries. A fine scale Widmanstätten colony microstructure was consistent throughout the structure within grains elongated parallel to the axis of epitaxy. Evidence of limited grain boundary α was detected, however, this was never continuous around individual grains. A moderate Burgers texture was measured employing EBSD, consistent with melt / cast titanium alloy forms cooling through the β transus.

Introduction

The high strength to weight ratio and damage tolerance characteristics of titanium alloys makes these systems attractive for applications such as large structural casing components, struts and vanes in the compressor sections of gas turbine engines, Figure 1. Such structures typically have integrated functionality, combining the needs to resist pressure loading with the requirement to provide local stiffening for attachment features whilst minimising excess mass. Creating load carrying sections

as webs, flanges and hollow features is possible using subtractive manufacture and fabrication or via casting with the use of cores, however, these methods show increasing cost and technological complexity[1] as the complexity of the geometry increases together with the requirements for precision on fine length scales. Using an additive manufacturing technique changes the balance point of these relationships[2], allowing potentially greater design sophistication[3] in shorter lead-time components. Moreover, the flexibility of the approach allows opportunities for economic savings through reduced processing operations, reduced component count or the use of simpler, lower cost preforms. In particular, additive processing can reduce the number of joints within complex structures. This can enable designs with increased stiffness while reducing the associated mass and feature cost of the joint regions.

Near net shape fabrication is a desirable outcome both through the substantial reduction of time spent in material removal, especially for complex forms, relative to machining intensive routes and also through the efficiency in material usage, particularly for high cost alloys. Castings can offer similar opportunities, although still requiring mould-making and core removal. However, key differences are in the requirements for the development of associated tooling such as patterns and metal running systems, particularly for intricate forms.

There are now many different types of additive process employing a variety of consumable and fusion techniques which display varying characteristics with respect to forming complexity, surface control, volumetric deposition rate, heat accumulation and feature resolution scale. Zheng et al[4] conducted a comparative evaluation of microstructures resulting from welding using tungsten inert gas (TIG), plasma and laser welded Ti 6Al 4V. All the processes produced weld beads without visual evidence of oxygen contamination when using local shielding arrangements. The titanium alloy showed differences in microstructure and hardness when welded using different processes. For these welding samples, a correlation between processing parameters and microstructure was established. This study showed that for laser welds, the grain size increased as the welding speed decreased. This is believed to correspond to residence time in the thermal region allowing grain coarsening for the heat affected zone, potentially combined with a reduced driving force for grain nucleation due to the reduced thermal gradients. Laser deposition is compared in

terms of heat input into the workpiece with TIG and plasma powder transferred arc (PTA) welding by Nowotny et al[5].

Due to the need to form narrow walls with sharp corners a blown powder deposition process was selected in preference to wire or tape based processes, which offer advantages in terms of material utilisation. Kobryn and Semiatin[6], gave an overview of laser additive manufacture for Ti 6Al 4V, showing that laser processes together with powder could yield comparative deposition rates to wire based processes. However, it is noted that deposition rate may be considered as the product of the voxel or bead cross-section and the process speed. The former term dictates the thermal momentum of the process in terms of the quantity of molten metal locally, which has substantial bearing on solidification rate, temperature gradients and associated distortions. The travel speed is typically limited by the need to maintain processing consistency particularly with direction changes, typically balancing machine manipulation kinematics with energy input rates due to the ballistic complexity in rapidly metering the consumable input rate without feed forward controls[7]. To allow fine feature resolution in blown powder systems, there are practical limitations to travel speed and pool size. With reducing pool dimension[8], the consumable input characteristics tend to scale accordingly[9-12] in ensuring stable melting. This scaling effect has practical and economic consequences through the increasing degree of processing involved in creating and precisely positioning finer scale wire consumables. For this reason powder consumables with diameters substantially below those available for drawn welding wires are favourable. Powder is not without drawbacks, however, for example through the need to maintain a coincident locus of adequate powder flux with a fine scale melt pool, unfused powder represents not only reduced yield, but also risks partially melted powder particles forming adherent agglomerates thus compromising surface finish and ultimately structural integrity. There are various techniques that have been proposed for controlling this[13] including further reducing travel speed, remelting passes which may be oblique to a surface and the use of secondary heat sources. Alternatively, the surface may be smoothed by mechanical or electro-chemical means.

In creating a complex geometry, invariably there will be regions of varying thermal accumulation, for example different cross-sections providing varying radiative and

convective cooling, bead start and stop points. For features with high curvature, internal and external edges will exhibit differences in surface processing rates for the same angular velocity. Due to the different radii, fine scale features depending on energy flux per unit length can be subject to variation. As Ti 6Al 4V develops a two phase microstructure the precise form of this structure will be very sensitive to temperature variations through the beta transus. Due to the comparatively small molten volumes at any point in time relative to the solidified form, the heat dissipation rate down thermal gradients close to the pool is typically rapid. The evolving microstructure will continue to be governed by the conditions in the adjacent solidified material and the spatial / temporal rate and duration of revisitations of a given volume by the molten region. A component exhibiting varying processing conditions at different locations throughout the geometry could risk significant microstructural and hence mechanical inhomogeneity. To accurately predict component performance under multi-axial service loading it is necessary to know any orientation effect on mechanical response. This is simplified if the metal structure can be controlled through process design to minimise crystallographic texture. Such texture could arise in the prior beta grains from epitaxial grain growth in the pool or competitive grain growth between layers along thermal gradients. Kobryn and Semiatin[6] studied the deposition of this alloy on a β-annealed substrate. They reported that the texture within the deposit partially corresponded to that of the substrate whilst also including a solidification induced <100> fibre[14]. The solidification texture could be expected to compete with the substrate texture with progressive height from the substrate. This would have implications for hybrid as opposed to complete additive fabrication. However this can also be interpreted that each layer and individual bead has the potential to reorient texture if toolpaths and deposition strategies are appropriately designed. Microstructural orientation could affect material anisotropy through alignment of grain boundaries. Texture in the beta grains is likely to be disrupted by heat input path variation[15] and timing. This may be achieved by manipulating the tool-path, for example using alternating, layer-wise cross-hatched volumetric fill techniques, side overlaps (which may vary in position particularly with perimeter outline and infill or chequerboard approaches) and discontinuous processing where the pool may be fully or partially extinguished and reinitiated. Texture may also arise from the hexagonal close packed α laths whose

textural variants are likely to be governed by the local thermomechanical conditions during the final passage of the volume of material through the β transus.

The current study did not aim to investigate the reduction of texture or the design of parameters to effect a columnar to equiaxed grain transition. Instead, it was intended to characterise the relative material homogeneity of a developmental structure made using available equipment at volumetric build rates representing those considered for commercial component fabrication.

Other researchers have noted a series of discernable bands[16], detectable as an etching response, corresponding in frequency and orientation to deposition layer intervals. These bands have been noted as a result of processing with different travel speeds, bead sizes and power levels in a range of additive processes for Ti 6Al 4V and have been modelled by Kelly et al[17]. For a high power, large pool size, high volumetric deposition rate 18kW CO_2 laser, it has been suggested that the effect is associated either with segregation effects during solidification or the thermal history[18]. Researchers at Birmingham University using a lower power (222-516W) and smaller spot size CO_2 laser (also used in blown powder laser deposition) noted that the bands were absent towards the top of the deposit [19]. Wu et al observed that these bands of varying etch response were linked to a variation in the size of the α laths, this was attributed to re-heating during subsequent passes of the laser. Their theory was that with an increasing number of layers for the same layer height the thermal mass above the β transus increases due to the reduced effectiveness of the substrate heat-sink with increasing intermediary cooling volume. From the authors' own experience, this effect also occurs in TIG shaped metal deposition in titanium as a pseudo steady state heat flux condition can be attained. These theories have more recently been demonstrated experimentally and through modelling[20].

The microstructure and properties of titanium alloys including temperature of the transus can be affected by interstitial content. This is clearly influenced by the consumable oxygen and moisture content and the degree of atmospheric shielding during processing. Inert atmospheres (usually argon) are needed to prevent oxygen and nitrogen pick up and subsequent embrittlement. Internal studies have shown that surface tension, which affects bead profile surface finish, can vary significantly with

titanium interstitial content. The cumulative time in the temperature sensitive region for high rate interstitial absorption must also be a consideration in process design. The standard of atmospheric protection will affect processing consistency and therefore can be expected to be a factor in the qualification of any process for structural applications in the aerospace industry.

As the basis for the current research, a three dimensional, thin-walled structure, produced from Ti 6Al 4V alloy using a direct laser deposition (DLD) technique was manufactured and then subjected to detailed metallographic examination. The structure was sectioned to provide six samples for characterisation. The original locations of these sections in relation to the complex DLD geometry are illustrated in Figure 2. These specific areas were selected because they provided samples of different wall thickness and examples of intersecting ligaments of different angular orientations. The resulting structures were then considered in light of the various processing conditions. The implications for service behaviour are also discussed.

Experimental Procedure

Specimens were extracted from the as processed DLD structure using mechanical cutting and subjected to a standard stress relief vacuum heat treatment typically applied to Ti 6Al 4V components (heat to 700°C at 55°C / hour, hold for 2 hours at 700°C and final cool to 20°C at 55°C / hour).

Each specimen was polished using standard metallographic techniques, and underwent a final chemical polish with an aqueous suspension of colloidal silica containing 20% H_2O_2 (hydrogen peroxide). This provided a surface finish of the required standard for electron back scatter diffraction (EBSD) analysis[21]. Prior to etching, specimens were examined under optical microscopy for evidence of porosity using a Reichart optical microscope with an attached Nikon CoolPix digital camera. Subsequently, specimens were etched with a solution of Krolls reagent (2% HF, 3% HNO_3, 95% distilled H_2O) for approximately 40 seconds. Microstructural analysis was performed on both a Jeol 6100 SEM and Phillips XL30CP SEM. High resolution

images of the microstructure were recorded using a HKL Flamenco software package attached to the Phillips SEM.

Three orthogonal sections were prepared from each specimen, to be described with reference to the co-ordinate system defined in Figure 2. Note the Z axis refers to the axis of material deposition.

Finally, Vickers hardness measurements were taken from each specimen employing an applied load of 10 Kg.

Results

Porosity

Micro-porosity was found to be widespread throughout the individual specimens, however, these very fine scale pores were typically less than 1μm in diameter. In specimen #4 (extracted at the mid length position of a relatively thin wall), a single 10 μm pore was detected. The largest example was found in specimen #6 at approximately 40 μm in diameter (this relates to an oblique intersection), Figure 3. Examinations from the orthogonal sections confirmed that the porosity was essentially equiaxed and not elongated in any preferred axis relative to the DLD epitaxy. No evidence of angular porosity or lack of fusion within the build pattern was detected.

Metallographic examination

A Widmanstätten type microstructure was observed in each of the specimens irrespective of wall thickness and local ligament geometry, Figures 4 & 5. The maximum α lath length was of the order of 5 μm, with thicknesses of approximately 1 μm. This type of structure is consistent with that seen in previous characterisations of welded forms of Ti 6Al 4V (including electron beam and TIG welds) and is common for the alloy immediately after cooling through the β transus (i.e. as cast and solidified but prior to subsequent working)[21].

Lower magnification optical microscopy was used to examine the prior β grain size, Figures 6 & 7, ranging from 0.1 mm up to approximately 1 mm. The Widmanstätten structure within these grains, however, was consistent. It should be noted, that there were slight deviations in the thickness of the α laths between individual prior β grains. However, there was no correlation of this coarsening with wall thickness or proximity to the outer surface of the structure.

Although the grains in Figures 6 and 7, representing the X-Y plane, appear essentially equiaxed, evidence of appreciable grain elongation was noted in the X-Z and Y-Z planes, Figure 8. This illustrates preferential grain growth parallel to the axis of DLD deposition. This is consistent with previous empirical evidence.

The potential for grain boundary α was of specific interest. Some examples were detected, Figure 9, however, these were infrequent and restricted to specimen #3. The α phase was never continuous around any single grain.

When inspected by eye, the external surface finish of the whole DLD component was notably rough. When viewed in section at high magnification, e.g. top and bottom edges in Figure 6, significant geometric irregularities were noted. It has been recognised that such re-entrant features on the surface could offer many potential sites for fatigue crack initiation should the component be aggressively loaded. Therefore, surface machining or acid pickling may be envisaged for eventual components. The current sections suggest that to completely eliminate this surface topography, approximately 0.5 mm of surface material would require removal. It can be confirmed that no α case was evident on the component surfaces.

EBSD mapping was also employed to characterise crystallographic orientations and texture. Relatively large areas of sample #5 were scanned on the Y-Z plane in order to identify whether any localised areas of strong texture were apparent, along with providing a measure of the bulk material crystallographic orientation. Individual orientation maps sampled an area of approximately 0.6 x 0.5mm, using a step size of 2μm. Figure 10 shows three orthogonal pole figures (basal, type I prismatic and type II prismatic) which describe the crystallographic texture of the material. It can be seen that the measured texture is typical of material which has been processed above the

beta transus[22], with strong individual poles representing orientations favoured by the Burger's transformation. The fact that these poles lie slightly off-axis may be related to the axis of epitaxy of the specimen during DLD build-up. Figure 11 indicates that despite these strong poles, no large effective structural units appear to exist within the microstructure, which should be beneficial for fatigue performance[23].

Orientation maps were produced at 1mm intervals in both the Y and Z directions to investigate whether individual beads of deposited material showed variations in crystallographic texture. Although some minor rotation of the poles was seen about the X axis (out of the page), this was not significant and there was little evidence of significant change in microtexture. However, it was possible to distinguish the boundaries between deposited beads, Figure 12.

Hardness

Three Vickers hardness measurements together with the calculated average for each specimen are presented in Table 1. Clearly, good consistency is noted between the data irrespective of location in the component. These values are also consistent with typical values for Ti 6Al 4V[24] in either rolled plate or forged disc forms.

Discussion

Given that the current trials formed part of an early stage programme of process evaluation and selection, the structure examined could be considered as pre-optimised in terms of microstructural control. Despite this, the general findings appear to be encouraging. Throughout the metallographic sections, a minimal degree of porosity was noted and where evident individual pores were extremely fine scale, corresponding to the pin hole porosity[25] noted by Goodwin et al. Kobryn et al[14] also noted porosity in the gauge volume of mechanical test specimens, some of which was due to lack of fusion. Whilst only one pore of this type was found in the present study, it is recognised that this may be a statistical effect due to the volumetric distribution, the two dimensional technique used for assessment and the relatively small areas sampled. Three dimensional inspection techniques such as computed tomography could provide a more accurate measurement of actual porosity in such structures.

The microstructure was consistent at all the sampled locations, irrespective of wall thickness, orientation and local heat sink conditions. This compares favourably with casting processes for example. However, it is recognised that the DLD material requires detailed mechanical assessment alongside further process optimisation. In particular, this mechanical assessment must consider the potential for orientation effects that may result from the planar nature of the DLD build process. The crystal orientation maps for the current material, however, are encouraging in this respect, particularly the lack of textural variation along both the Y and Z directions. Whilst a transformation texture typical of β processing is evident, there is no strong textural alignment with either the X,Y or Z axes. As such, mechanical loading in any of these directions would probably show a minimal orientation effect. An evaluation of mechanical properties of the current material would be required to validate these theories. The fact that no large effective structural units, which could prove detrimental to fatigue properties, were evident is also encouraging. However, it should also be noted that Kobryn[14] et al found evidence of anisotropic yield strength, fatigue response and an unusual planar response associated with porosity for compact tension samples. This planar porosity was also found in the work by Groh[26].

The preferred epitaxy within prior β grains, with grains elongated parallel to the axis of build, is consistent with previously reported studies[25, 14]. This is an important feature to note given the deliberate complexity of build pattern employed during the current trials in contrast to some of the simpler forms of test geometries reported by previous authors. Ultimately, it can be presumed that the β transus isotherm generated during the current process must have remained essentially perpendicular to the build axis. The complex interaction of tool-path, molten pool volume, depth, time period and percentage of overlap and cooling duration will affect this isotherm. Specific control of either of these variables could be considered in an attempt to influence the alignment and pattern of grain orientations. Control would need to be in relation to a validated process model for microstructural generation and could be via finite element approaches[27,28], where each cell has phase transformation information, or reverse engineered from measured process data.

The size of the prior β grains (i.e. maximum length parallel to the build axis) was similar to those reported by Kobryn and Semiatin using a much more powerful laser source with increased melt pool and presumably decreased freezing rate[14]. Grain width and porosity population appear to be finer. The β grain morphology is controlled by the combination of the thermal gradient and the cooling rate. The solidification velocity is related to the thermal gradient and cooling rate by –

$$R = \frac{1}{G} . \frac{\delta T}{dt} \quad (1)$$

where R is the solidification velocity, G the thermal gradient and δT/dt the cooling rate[29]. The thermal gradient is a function of the previous layer and the bead heat retention and also the bead size of the successive layer, i.e. the local molten mass and the processing rate. The evolved substrate temperature will be in a process control range limited by economic processing rate and also the danger of excess heat localisation, which may cause morphological coarsening and potentially also distortion. This clearly indicates that additional parameters such as those already discussed are important in controlling grain morphology and size[30]. The morphology of the α laths has previously been modelled for wire based deposition[31,32]. It is pertinent to compare these microstructures to those evolved from competing cast processes. The latter will tend to produce relatively large, equi-axed grains encompassing relatively coarse α laths at > 5 microns. This lath size is typically reduced in forged Ti 6Al 4V variants at approximately 1-2 microns. The lath size in the present examples was restricted to approximately 1 μm and can be compared with the near equiaxed-like morphology with a smaller aspect ratio of α laths described by Dinda et al[33]. Thus, the additive process clearly generates refined microstructure which in turn should offer benefits to mechanical strength and fatigue.

With regard to the banding seen by other researchers with similar conditions, the authors have seen this effect in SMD using TIG processes. Others[34] have seen this as a banded variation in reflectivity for microsamples from material formed via laser diode and wire Ti 6Al 4V deposition. That such an effect was not observed in this study may be due to the thermal processing rate, particularly the isotherm velocities being substantial, and the interpass temperature, time, remelting and recrystallisation

allowing sufficient solid phase diffusion of any concentrated α-strengthening elements to be dispersed.

From a compositional viewpoint, X-ray spectrographic measurements of local chemistry were consistent at randomly chosen sites throughout the structure. Previous workers have postulated episodes of local segregation due to variations in elemental density and distribution within the melt pool. Variable heat concentrations with successive beads and stop-start events may also lead to volatilisation[35] of specific elements (e.g. aluminium and vanadium). This does not appear to be evident in the current material, however, the resolution of the EDX equipment may not be sufficient to detect the effect. However, the consistent α lath sizes noted throughout the structure do not support any great variation on local chemistries, either due to issues of buoyancy or variable superheat. Within the grain structure, only sporadic examples of isolated grain boundary α were noted, consistent with relatively fast cooling rates. Together with the absence of surface α case this would be considered beneficial to subsequent high cycle fatigue properties.

Although minor examples of porosity were found, the source of this porosity is difficult to define. However, it should be noted that even individual sourced powder particles can contain gas entrapment features due to the instabilities of the atomisation process, Figure 13[36]. Blown powder deposition allows component manipulation, although toolpath trajectories over complex contours may not always be perpendicular to gravity. Process conditions may affect pool fluidity, pool shape and process rate, hence time for floatation. Removing the argon shielding gas, as done in electron beam based deposition would remove a possible source of porosity. Deposition at reduced pressure would be expected to increase the intensity of nucleation of gas bubbles and also allow greater vaporisation of metallic elements whereas a higher pressure would make porosity more difficult. Shallow pools restrict the metallostatic pressure, which can limit bubble stability, this may mean that other factors being equal, there would be an increased number of pores for the same volume when created from a fine build technique as observed in the current material.

All current hardness measurements were slightly above those previously reported[37] for the higher deposition rate 'AeroMat' material. This may be explained by the faster cooling indicated by the finer microstructure of the samples examined in this study. This comparative result supports the modeled findings of Qian et al [18, 38], who reported that for the same volumetric form, created with varying build up rates through changing the pool voxel dimensions with similar processing speeds, there is a linkage of cooling rate to pool size. The surface finish seen in this study did not approach that reported elsewhere[39] (7-7.5 μm Ra). Clearly the surface finish will affect process rate, yield and the need for and degree of subsequent processing before inspection and final condition of use is achieved. Refinement of this issue is clearly necessary to achieve optimum in service material conditions.

Conclusions

- The DLD component contained a low volume of spherical micro-porosity, with pore diameter <1μm. The single largest pore found within the structure was approximately 40 μm in diameter.
- The material contained a Widmanstatten microstructure, characteristic of cooling from above the β transus. The α laths within the Widmanstatten microstructure were approximately 5 μm long and 1 μm thick. Only minor variations in these dimensions were noted between individual prior β grains.
- Grain elongation was noted parallel to the axis of DLD epitaxy / build up. Limited grain boundary α was detected, although never continuous around any particular grain.
- EBSD analysis confirmed a moderate Burgers texture within the microstructure, typical of a cast titanium alloy cooling through the β transus. However, the microstructure was found to be more uniform than a comparable casting, which may have implications for mechanical response and volumetric inspection

Acknowledgements

The authors would like to acknowledge the financial and technical support of Rolls-Royce plc in the production of this work.

References

[1] K. G. Swift, J. D. Booker, Process Selection, (2nd Edition). Butterworth-Heinemann, Oxford, UK, 2003 pp. 300

[2] L. Xue, A. Theriault, B. Rubinger, D. Parry, F. Ranjbaran and M. Doyon, Proceedings of the 22nd International Congress on Applications of Lasers and Electro-Optics 2003. Published on CD ROM.

[3] L. Xue, A. Theriault, M.U. Islam, M. Jones, H.-P. Wang, Proceedings of the 23rd International Congress on Applications of Lasers and Electro-Optics 2004. Published on CD ROM.

[4] S. Zheng, P. Dayou, Z. Weihong, T.Y. Kuang. SIMTech Technical Report. (PT/01/015/JT). Singapore Institute of Manufacturing Technology. Joining Technology Group. Process Technology Division. 2001. www.simtech.a-star.edu.sg/Research/TechnicalReports/TR0120.pdf

[5] S. Nowotny, S. Scharek, E. Beyer, K.H. Richter, Journal of thermal spray technology, Vol.16 No.3, 2007, pp. 344-348

[6] P.A. Kobryn and S.L. Semiatin "The Laser Additive Manufacture of Ti-6Al-4V" (Overview), September 2001, pp. 40-42.

[7] Y. Li, H. Yang, X. Lin, W. Huang, J. Li and Y Zhou, Materials Science and Engineering A360, 2003, pp. 18-25.

[8] J. Kim, Y. Peng, Journal of Materials Processing Technology Vol.104, 2000, pp. 284-293.

[9] A. Pinkerton and L. Li, Journal of Engineering Manufacture, Vol 218, 2004, pp. 363-374.

[10] A.J. Pinkerton and L. Li, Journal of Manufacturing Science and Technology, Vol.126 No.1, 2004, pp. 34-42.

[11] A.J. Pinkerton and L. Li, International Journal of Machine Tools and Manufacture, Vol44 No.6, 2004, pp. 573-584.

[12] A. Pinkerton and L. Li, Journal of Mechanical Engineering Science, Vol.218 No.6, 2004, pp. 531-541.

[13] J.Lawrence and L.Li, Journal of Laser applications, Vol.14, no.2, (May 2002), pp. 107-113.

[14] P.A. Kobryn, S.L. Semiatin, In proc. conf. Solid Freeform Fabrication Symposium 2001, ed.s D.L.Bourell, J.J.Beaman, R.H.Crawford, H.L.Marcus, K.L.Wood, J.W.Barlow, publ. by The Univ. of Texas at Austin, Texas, USA, 2001, pp. 179-186.

[15] C. Hu and T.N. Baker, Metallurgical and Materials Transactions, A. Vol 27A, 1996, pp. 4039-4047

[16] B. Baufeld, O. van der Biest, R. Gault, AEROMAT 2008, ASM International, 23-26 June 2008, Austin Texas, USA. Published on CD-ROM

[17] S.M. Kelly and S.L. Kampe, Metallurgical and materials transactions. A, Vol. 35, No 6, 2004, pp. 1869-1879.

[18] S.M. Kelly, S.L. Kampe, C.R. Crowe, In proc. conf. Solid Freeform and Additive Fabrication – 2000, compiled by S.C.Danforth, D.Dimos, F.B.Prinz, publ. by MRS, USA, 2000, pp. 3-8.

[19] P.S. Goodwin, C. Mitchell, J. Liang, J.M. and X. Wu, In proc. conf. Metal Powder Deposition for Rapid Manufacturing 2002, compiled by D. Keicher, J.W. Sears, J.E. Smugeresky, publ. by MPIF, 2002, pp. 87-94.

[20] L. Qian, J. Mei, X. Wu, Materials science, 2007, vol. 539-43 (4), pp. 3637-3642.

[21] F. Wagner, N. Bozzolo, O. van Landuyt and T. Grosdidier, Acta Materialia, Vol. 50, 2002, pp. 1245-1259.

[22] G. Lutjering, Material Science & Engineering A243, 1998 pp. 32-45.

[23] M.T. Whittaker, W.J. Evans, R. Lancaster, W. Harrison, P.S. Webster. International Journal of Fatigue, Vol. 31 Nos.11-12, 2009, pp. 2022-2030.

[24] S.R. Tuppen, M.R. Bache, W.E. Voice, International Journal of Fatigue, Vol. 27 No. 6, 2005, pp. 651-658.

[25] P.S. Goodwin, C. Mitchell, J. Liang, J. Mei and X. Wu, Proceedings of Metal Powder Deposition for Rapid Manufacturing, , San Antonio Texas, USA, 8-10th April, 2002, pp. 87-94.

[26] C. Henry III., NASA/TM—2006-214256, 2006. http://gltrs.grc.nasa.gov/ reports/2006/TM-2006-214256.pdf

[27] L-E Lindgren “Computational Welding Mechanics”, CRC Press, 2007.

[28] A. Crespo, A. Deus, R. Vilar, Paper 2005, ICALEO 2006, http://www.lia.org/store//ICAL06_2005.

[29] N.W. Klinbeil, C.J.Brown, S. Bontha, P.A. Kobryn, H.L. Fraser, Proceedings of the Solid Freeform Fabrication Symposium, 2002, University of Texas, Austin, USA, pp.142-149.

[30] S.M. Kelly, S.S. Babu, S.A. David, T. Zacharia and S.L. Kampe, in 7th International Conference on Trends in Welding Research, May 16-20, 2005, Pine Mountain, GA, USA, 2005, pp. 65-70.

[31] C. Charles, N. Järvstråt, 8th International Conference on Trends in welding research, Pine Mountain, Georgia, June 2-6, 2008. Published on CD-ROM.

[32] C. Charles and N. Järvstråt, Proceedings of the 11th World Conference on Titanium Kyoto, Japan, 2007, pp 1201-1204.

[33] G.P. Dinda, L. Song, and J. Mazumder, Met. Mat. Trans. A, Vol. 39A, 2008, pp. 2914-2922.

[34] S.D. Sharples, M. Clark, W. Li, M.G. Somekh 1st International Symposium on Laser Ultrasonics, Science, Technology and Applications, July 16-18 2008, Montreal, Canada. http://www.ndt.net/article/laser-ut2008/papers/Sharples%20LU2008.

[35] C.L. Lach, K.M. Taminger, AEROMAT 2008, ASM International, 23-26 June 2008, Austin Texas, USA. Published on CD-ROM.

[36] J. Forsdike, MRes Thesis, Swansea University, 2006.

[37] L. Qian, J. Mei, and X. Wu, “The Influence of position and laser power on the thermal history in a direct laser fabricated Ti alloy”, Mat. Sci. & Tech, Vol. 21 No. 5, 2005, pp. 597-605.

[38] L. Qian, J. Mei, and X. Wu, Materials Science Forum, Vol 539-543, 2007.

[39] Xue, L., J.-Y. Chen, and A. Theriault, “Laser Consolidation of Ti-6Al-4V Alloy for the Manufacturing of Net-Shape Functional Components”, Proceedings of ICALEO' 2002, Scottsdale, Arizona, USA, October 14-17, 2002, pp. 169-178.

Table 1. Vickers hardness measurements.

	Indentation #1	**Indentation #2**	**Indentation #3**	**Average Hv**
Specimen #1	367	377	380	***375***
Specimen #2	381	372	375	***376***
Specimen #3	366	365	373	***368***
Specimen #4	367	360	357	***361***
Specimen #5	369	377	373	***373***
Specimen #6	376	360	360	***365***

Figures

Figure 1: (a) Complete additive manufactured component (b) feature addition. Note that each component demonstrates examples of arc heat source and wire consumable shape metal deposition structures, minimising five-axis mill-turn machining centre requirements.

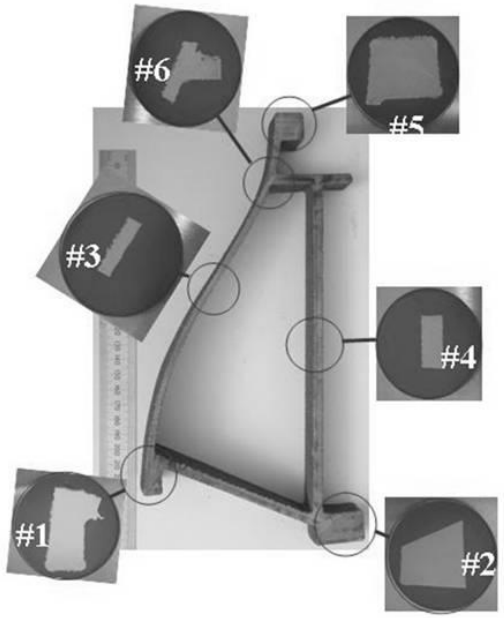

Figure 2: DLD structure with locations for the six metallographic specimens. The axis of epitaxy (Z) is out of page.

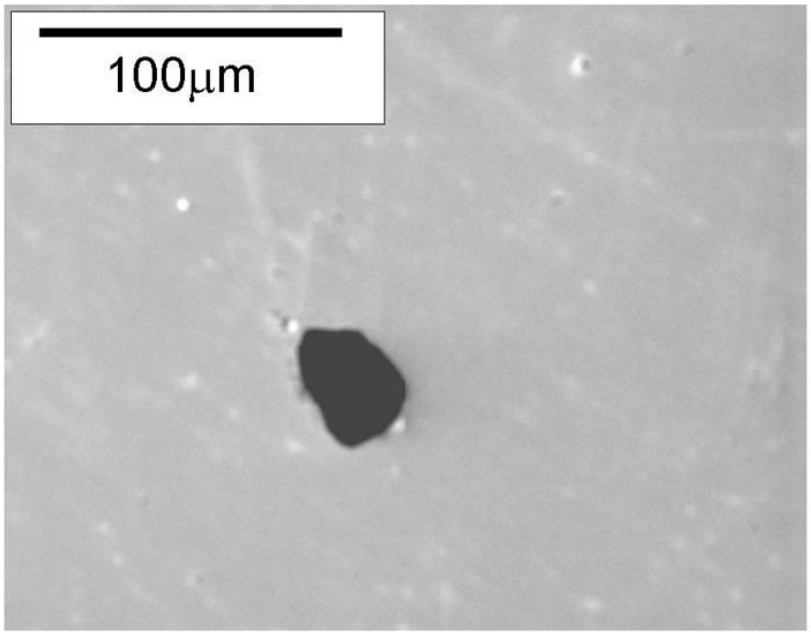

Figure 3. Relatively large pore in specimen #6.

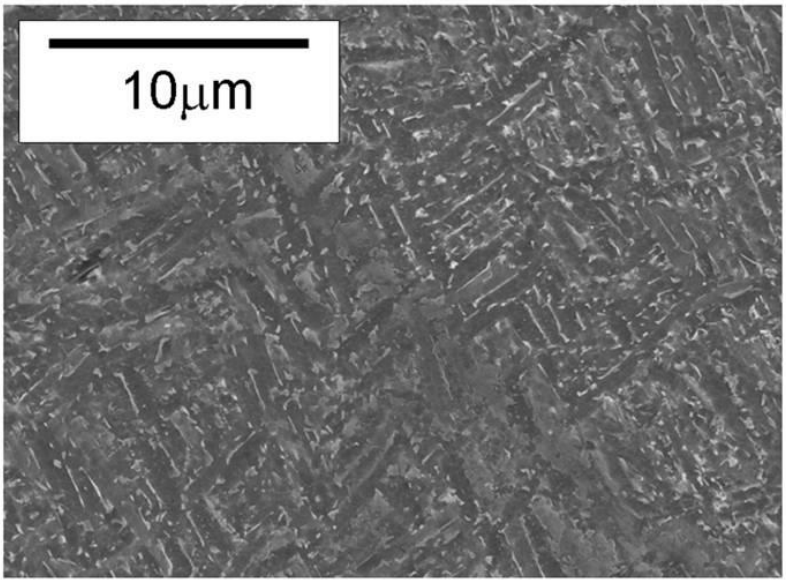

Figure 4. High resolution SEM mage of Ti 6Al 4V microstructure, specimen 6, X-Y plane.

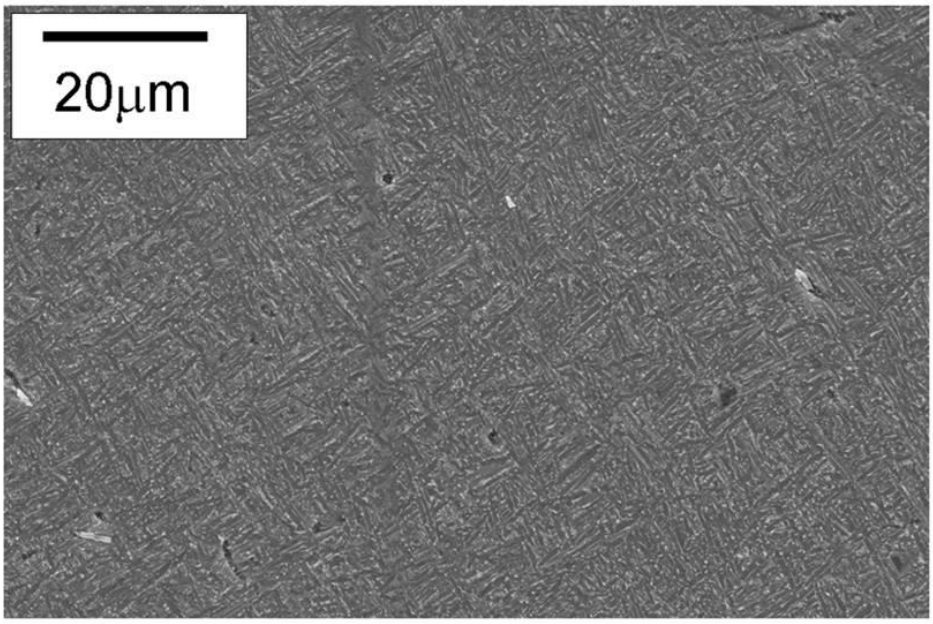

Figure 5. SEM image of Ti 6Al 4V microstructure, specimen 6, X-Y plane.

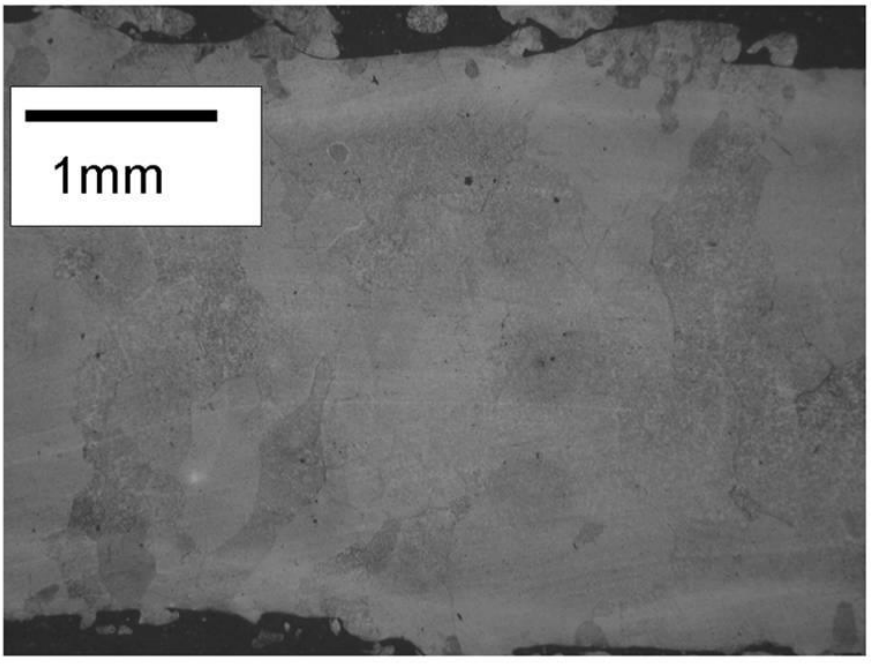

Figure 6. Grain structure within Ti 6Al 4V DLD thin wall section, specimen #1, X-Y plane.

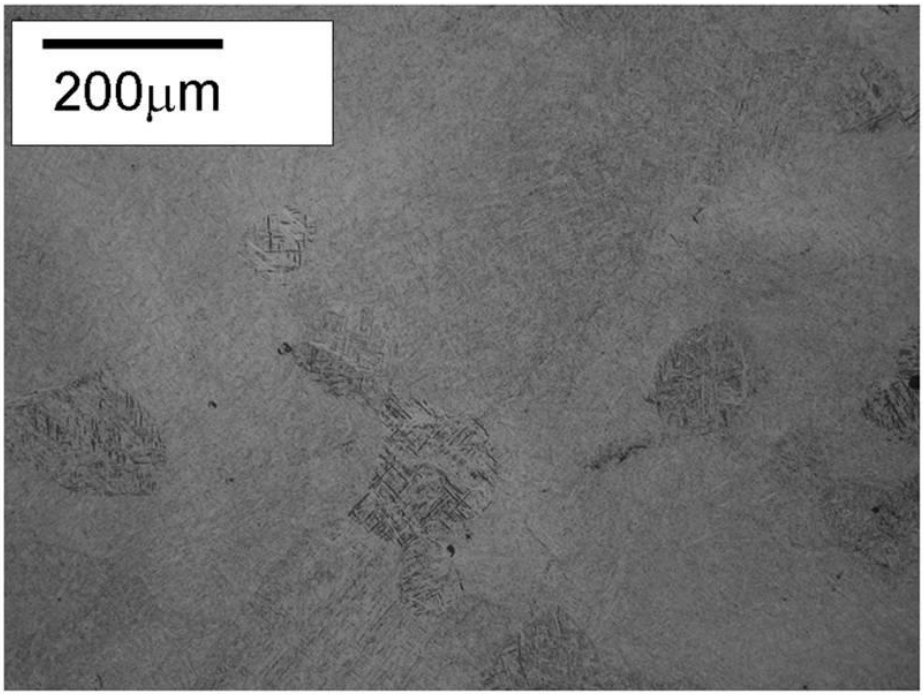

Figure 7. Grain structure of Ti 6Al 4V in a relatively thick wall location, specimen #1, X-Y plane.

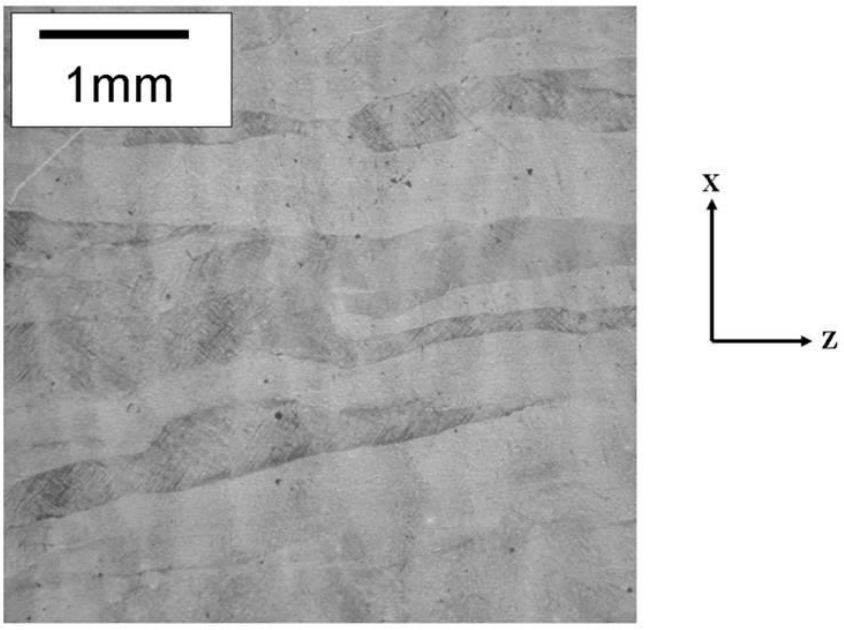

Figure 8. Preferred grain growth viewed on the X-Z plane, specimen #3.

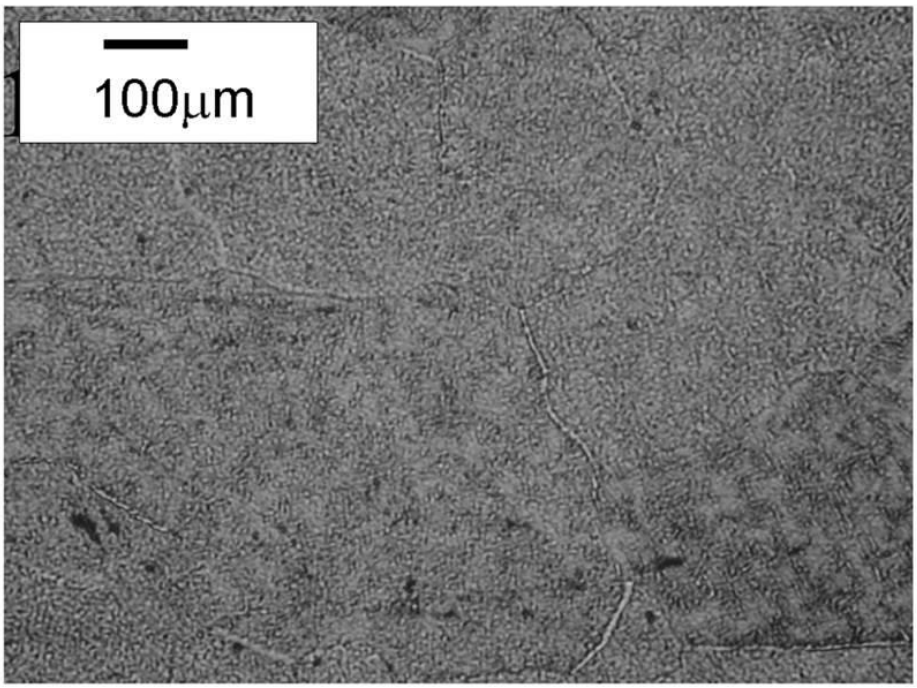

Figure 9: Discontinuous grain boundary α specimen 3 X-Y plane.

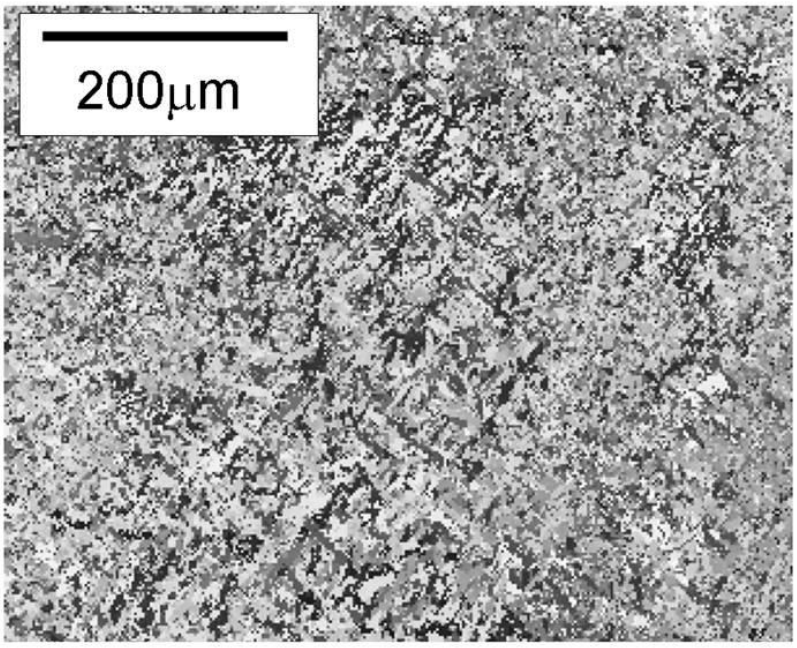

Figure 10: EBSD orientation map from specimen #5, area of map 600 x 500 μm.

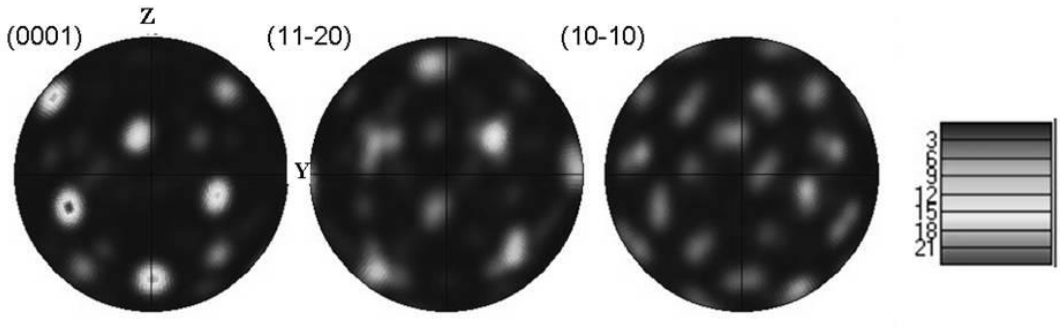

Figure 11: Basal {0001} pole figure for specimen #5, X axis out of the page.

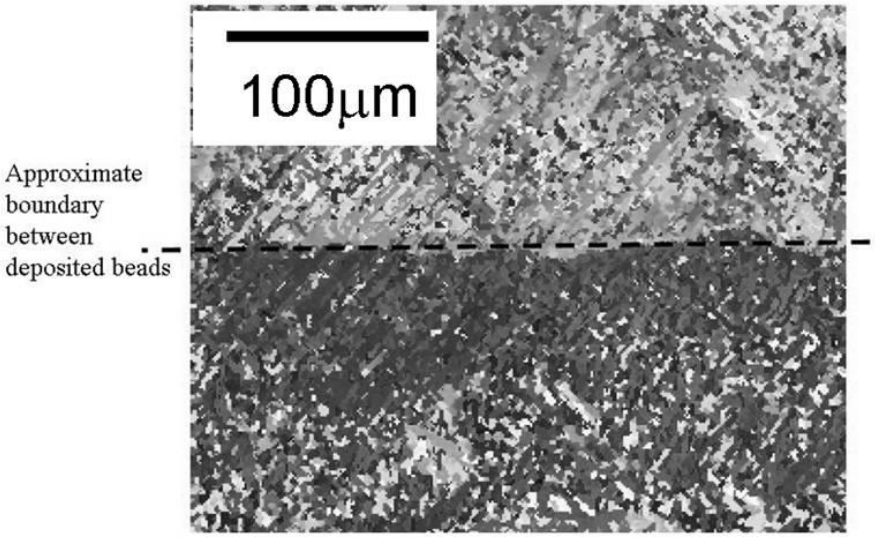

Figure 12: EBSD orientation map from specimen #5, indicating boundary between the β transformed region of 2 deposited beads. Area of map 600 x 500 μm.

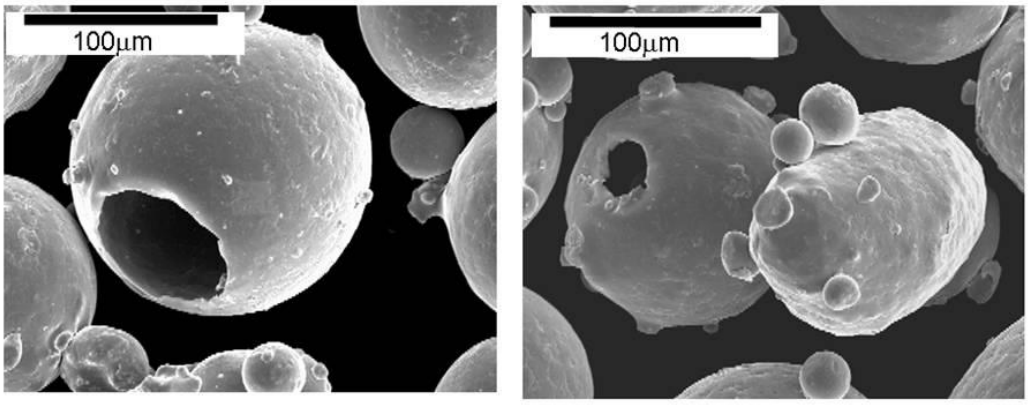

Figure 13: Gas entrapment features in powder stock.